A Planar Microstrip Crossover With Lumped Inductors for Three Intersecting Channels

Lin-Sheng Wu, *Member, IEEE*, Yong-Xin Guo, *Senior Member, IEEE*, and Jun-Fa Mao, *Fellow, IEEE*

***Abstract*—A planar microstrip crossover is proposed by using a stub-loaded ring structure with lumped inductors to realize good transmission and isolation performances for three intersecting channels. It can take the place of three conventional dual-channel crossovers. Since the component is with a sixfold rotational symmetric configuration, it can be analyzed by using its eigen-admittances and the even-/odd-mode theory. The analytical equations are derived to generate the design curves to determine the circuit parameters, operating bandwidth and transmission phase. The influence of the utilized lumped inductors on the crossover performance is also considered. A prototype is developed at 1.0 GHz with an occupied area of $0.308 \times 0.294\ \lambda_g^2$, where λ_g is the guided wavelength of the central frequency. The performances of diagonal transmission, port matching, and isolation between different channels are achieved with a 6% operating bandwidth, which has been demonstrated by the theoretical, simulated, and measured results.**

***Index Terms*—Eigen-admittance, lumped inductor, planar microstrip crossover, sixfold rotational symmetric structure, three intersecting channels.**

I. Introduction

CROSSOVER has become an important type of passive component in various microwave circuits due to the rapid development of high-density microwave integrated systems. 3-D structures, such as an air-bridge, a via-hole, and a multilayer circuit [1], [2], can be used to separate two intersecting signal channels, but they also increase the fabrication cost and introduce parasitic effects, especially for high frequencies. A broadband via-less crossover is proposed in [3] by using microstrip to coplanar waveguide (CPW) transitions, where the CPW is realized on the ground plane of the microstrip line. Two orthogonally placed conductor-backed CPWs are used to build up a compact crossover [4], where both the top and bottom metal planes of a printed circuit board (PCB) are with traces and connected by via-holes. Combining a pair of two-port microstrip-to-slotline transitions and a pair of four-port ones, two crossing signal paths with low insertion loss and high isolation are achieved [5]. Although all the crossovers in [3]–[5] can operate with large bandwidths by using both sides of one substrate simultaneously, their etched grounds avoid the direct stacking on other circuits in an integrated system. Therefore, fully planar crossovers with a complete ground plane are in demand.

Two branch-line hybrid couplers are first combined for crossover application [6]. The matched four-port ring-cross structure [7] has been proven to be able to work as a planar crossover [8]. It can also be realized with a symmetric four-port annular ring [9]. Various branch-line structures are proposed to provide 0-dB directional coupling for crossovers with different bandwidths [10]–[12]. Stub-loaded multi-section branch-line couplers are also attractive candidates [13], [14]. In [15]–[17], double rings connected by four line sections are used to achieve good crossover performance within an operating bandwidth of about 20%, even for two intersecting signal channels with arbitrary characteristic impedances. A compact unit cell is proposed with lumped elements in [18] to construct directional couplers and crossovers, which are further applied into a 4×4 Bulter matrix. In [19], a half-wavelength square patch and its fractal counterparts are used in planar crossovers. In [20], a broadband crossover is built up with the combination of a ring resonator and circular patch. Recently, the design of a crossover operating within dual bands has drawn much attention [21]–[25]. Two dual-band crossovers have been successfully implemented by using a trisection branch-line coupler and its stub-loaded modification [21], [22]. It is exactly validated in [23] and [24] that two-section branch-line structures also provide enough design freedom for dual-band crossover applications when loading stubs are incorporated. By introducing open- and short-ended stubs into the symmetric structure first proposed in [10], the crossover performance is extended from a single band to dual operating bands [25].

It is noticed that all the above-mentioned crossovers are for two intersecting signal channels. When three channels cross each other in the layout, three dual-channel crossovers can be used, as shown in Fig. 1(a). However, the overall size of this complicated crossover section may be large, especially for low frequencies. Therefore, a compact component for a tri-channel crossover, as shown in Fig. 1(b), is still desired.

On the other hand, the symmetric six-port coupler [26] is a suitable multiport component for the application of a six-port

Manuscript received November 27, 2013; revised February 15, 2014; accepted February 21, 2014. Date of publication March 13, 2014; date of current version April 02, 2014. This work was supported by the Singapore Ministry of Education Academic Research Fund Tier 1 Project R-263-000-667-112, the National University of Singapore (Suzhou) Research Institute under Grant NUSRI-R-2012-N-010, the Natural Science Foundation of Jiangsu Province, China, under Grant BK20131190, and the National Natural Science Foundations of China under Grant 61370008.

L.-S. Wu is with the Department of Electrical and Computer Engineering, National University of Singapore, Singapore 117583, Singapore, and also with Key Laboratory of Ministry of Education for Design and Electromagnetic Compatibility of High-Speed Electronic Systems, Shanghai Jiao Tong University, Shanghai 200240, China (e-mail: wallish@sjtu.edu.cn).

Y.-X. Guo is with the Department of Electrical and Computer Engineering, National University of Singapore, Singapore 117583, Singapore, and also with the National University of Singapore (Suzhou) Research Institute, Suzhou, Jiangsu Province 215123, China (e-mail: yongxin.guo@nus.edu.sg).

J.-F. Mao is with the Key Laboratory of Ministry of Education for Design and Electromagnetic Compatibility of High-Speed Electronic Systems, Shanghai Jiao Tong University, Shanghai 200240, China (e-mail: jfmao@sjtu.edu.cn).

Color versions of one or more of the figures in this paper are available online at http://ieeexplore.ieee.org.

Digital Object Identifier 10.1109/TMTT.2014.2309558

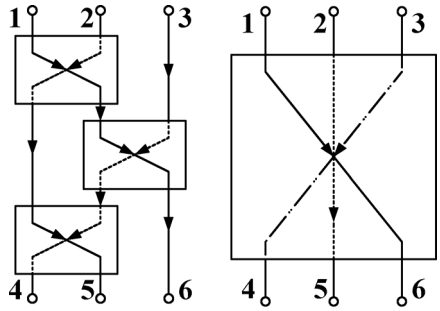

Fig. 1. Diagrams of: (a) the combination of three dual-channel crossovers for three intersecting channels and (b) a tri-channel crossover.

reflectometer in a network analyzer [27]. Some simple configurations are proposed for this purpose, such as a matched junction [28], a ring [29], and a ring-star structure [30]. In order to increase the bandwidth of a six-port coupler, a complicated topology of double rings with an inside star is presented in [31], and it is further modified in [32]. A six-port symmetric decoupling network is presented for a circulant symmetric six-element antenna array [33]. When the coupling between diagonal ports is close to 0 dB, the symmetric six-port coupler can work as a tri-channel crossover. However, no prototype has been developed until now that meets the requirement of 0-dB diagonal coupling with a simple planar configuration.

In this paper, a planar crossover is proposed for three intersecting signal channels, which is based on a six-port ring connected with six lumped inductors through transmission lines. The critical parameters of the compact component are designed by using the eigen-admittances of the six-port network, which are calculated with the even-/odd-mode theory. The achievable fractional bandwidth is explored within the selectable range of parameters. The influence of a Q-factor and tolerance of lumped inductors is also discussed. A microstrip prototype is designed to validate our method. Reasonable agreement is obtained among the theoretical, simulated, and measured responses.

II. Sixfold Rotational Symmetric Structure for Tri-Channel Crossover

A sixfold rotational symmetric reciprocal structure with six ports is shown in Fig. 2. Its Y-matrix can be written as

$$\mathbf{I} = \mathbf{YV} = \begin{bmatrix} a & b & c & b & c & d \\ b & a & b & c & d & c \\ c & b & a & d & c & b \\ b & c & d & a & b & c \\ c & d & c & b & a & b \\ d & c & b & c & b & a \end{bmatrix} \mathbf{V} \tag{1}$$

where a is the self-admittance of each port and b, c, and d are the mutual admittances between different ports. Since there are only four independent elements in the Y-matrix, it can be diagonalized with eigenvalue decomposition as

$$\mathbf{Y} = \mathbf{P}\mathbf{\Lambda}\mathbf{P}^{-1} \tag{2}$$

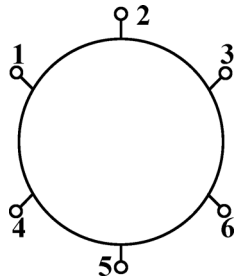

Fig. 2. Diagram of a sixfold rotational symmetric structure with six ports.

where

$$\mathbf{\Lambda} = \text{diag}\left\{ \begin{matrix} a-2b+2c-d, a+2b+2c+d, \\ a+b-c-d, a+b-c-d, \\ a-b-c+d, a-b-c+d \end{matrix} \right\} \tag{3}$$

$$\mathbf{P} = \begin{bmatrix} -1 & 1 & 0 & -1 & 0 & 1 \\ 1 & 1 & -1 & 0 & 1 & 0 \\ -1 & 1 & -1 & 1 & -1 & -1 \\ 1 & 1 & 1 & -1 & -1 & -1 \\ -1 & 1 & 1 & 0 & 1 & 0 \\ 1 & 1 & 0 & 1 & 0 & 1 \end{bmatrix}. \tag{4}$$

The eigen-voltage $\mathbf{V}'$ and current $\mathbf{I}'$ are then given by

$$\begin{aligned} \mathbf{W}' &= 6\mathbf{P}^{-1}\mathbf{W} \\ &= \begin{bmatrix} -W_1+W_2-W_3+W_4-W_5+W_6 \\ W_1+W_2+W_3+W_4+W_5+W_6 \\ -W_1-2W_2-W_3+W_4+2W_5+W_6 \\ -2W_1-W_2+W_3-W_4+W_5+2W_6 \\ -W_1+2W_2-W_3-W_4+2W_5-W_6 \\ 2W_1-W_2-W_3-W_4-W_5+2W_6 \end{bmatrix} \end{aligned} \tag{5}$$

where the vectors $\mathbf{W}$ and $\mathbf{W}'$ can be replaced by $\mathbf{V}$ (or $\mathbf{I}$) and $\mathbf{V}'$ (or $\mathbf{I}'$), respectively, and the elements $W_i (i = 1, 2, \ldots, 6)$ can be replaced by V_i or I_i correspondingly.

The eigen-admittances are defined with the six-port network excited by the eigen-voltages and currents. For the topology shown in Fig. 2, if each sixth part of the network is symmetric itself, the simplified circuits can be derived by the eigen-excitations in (5). According to the symmetries of the network and the combined excitations, electric and magnetic walls are introduced into the network, as shown in Fig. 3. The six-port network is then converted into several single- or two-port subnetworks.

The first two eigen-admittances $a-2b+2c-d$ and $a+2b+2c+d$ are just equal to the input admittances Y_{ooo} and Y_{eee} of the single-port sixth subnetworks shown in Fig. 3(a) and (b) with all the symmetric planes set to electric and magnetic walls, respectively.

It is noticed that the two-port fourth subnetwork in Fig. 3(c) has the same Y-matrix $\mathbf{Y_{oe}}$ as the subnetwork in Fig. 3(d). Therefore, they correspond to the same eigen-admittance $Y_{oe} = a+b-c-d$. According to the combined excitation of the left upper fourth subnetwork in Fig. 3(c), we have

$$\begin{bmatrix} -I_1 \\ -I_1 \end{bmatrix} = \begin{bmatrix} Y_{11,oe} & Y_{21,oe} \\ Y_{21,oe} & Y_{22,oe} \end{bmatrix} \begin{bmatrix} -V_1 \\ -2V_1 \end{bmatrix}. \tag{6}$$

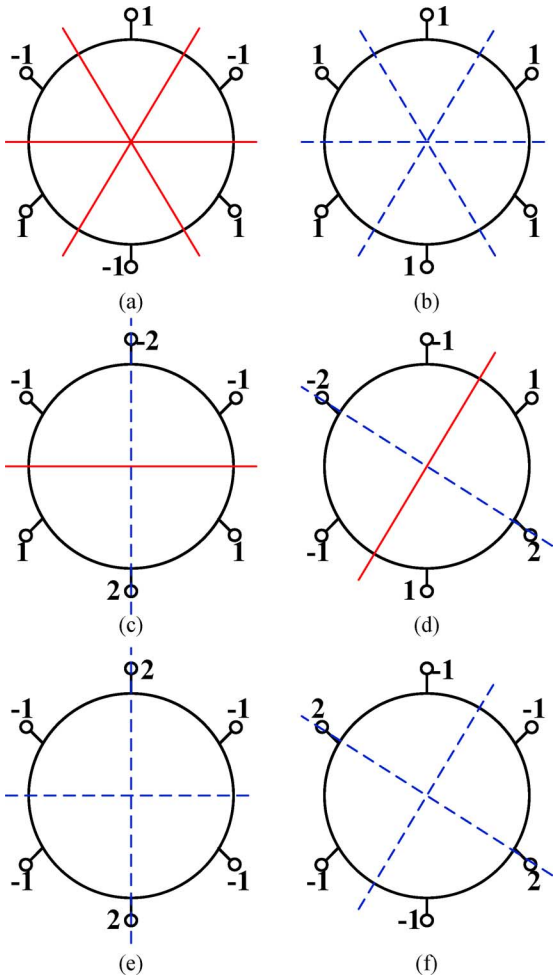

Fig. 3. Subnetworks of the sixfold rotational symmetric network under the eigen-excitations and with the symmetric planes, where the numbers near the ports are the corresponding coefficients in (5), and the red solid and blue dashed lines (in online version) correspond to electric and magnetic walls, respectively.

Note that the coefficients of the current and voltage correspond to the eigen-excitation with electric and magnetic walls. It is derived from (6) that

$$Y_{oe} = I_1/V_1 = Y_{11,oe} + 2Y_{21,oe} = Y_{21,oe} + 2Y_{22,oe}. \quad (7)$$

For the proposed symmetric structure, it is found that

$$Y_{11,oe} + Y_{21,oe} = 2Y_{22,oe}. \quad (8)$$

Similarly, the two-port fourth subnetworks in Fig. 3(e) and (f) correspond to the same Y-matrix $\mathbf{Y_{ee}}$ and the same eigen-admittance $Y_{ee} = a - b - c + d$. According to the combined excitation of the left upper fourth subnetwork in Fig. 3(e), we have

$$\begin{bmatrix} -I_1 \\ I_1 \end{bmatrix} = \begin{bmatrix} Y_{11,ee} & Y_{21,ee} \\ Y_{21,ee} & Y_{22,ee} \end{bmatrix} \begin{bmatrix} -V_1 \\ 2V_1 \end{bmatrix}. \quad (9)$$

The eigen-admittance is given by

$$Y_{ee} = I_1/V_1 = Y_{11,ee} - 2Y_{21,ee} = -Y_{21,ee} + 2Y_{22,ee} \quad (10)$$

where

$$Y_{11,ee} - Y_{21,ee} = 2Y_{22,ee}. \quad (11)$$

Note that (8) and (11) are guaranteed by the symmetry of the six-port structure. When the four eigen-admittances Y_{ooo}, Y_{eee}, Y_{oe} and Y_{ee} are calculated, the elements a, b, c, and d can be solved. The whole Y- and S-matrices of the six-port symmetric network are then determined.

If the sixfold rotational symmetric structure is applied to realize a perfect crossover for three intersecting signal channels, its S-parameters should satisfy

$$\mathbf{S} = \begin{bmatrix} 0 & 0 & 0 & 0 & 0 & e^{-j\varphi_0} \\ 0 & 0 & 0 & 0 & e^{-j\varphi_0} & 0 \\ 0 & 0 & 0 & e^{-j\varphi_0} & 0 & 0 \\ 0 & 0 & e^{-j\varphi_0} & 0 & 0 & 0 \\ 0 & e^{-j\varphi_0} & 0 & 0 & 0 & 0 \\ e^{-j\varphi_0} & 0 & 0 & 0 & 0 & 0 \end{bmatrix} \quad (12)$$

where φ_0 is the undetermined transmission phase of each channel. The Y-matrix is obtained from the S-matrix by

$$\mathbf{Y} = \frac{1}{Z_0}(\mathbf{U} - \mathbf{S})(\mathbf{U} + \mathbf{S})^{-1} \quad (13)$$

where $Z_0 = 50\ \Omega$ is the port impedance, and $\mathbf{U}$ is a unit matrix. Combining (12) and (13) and then comparing with (1), we have

$$a = -j\frac{\cot\varphi_0}{Z_0} \quad (14)$$

$$d = j\frac{\csc\varphi_0}{Z_0} \quad (15)$$

$$b = c = 0. \quad (16)$$

Substituting (14)–(16) into (3), the eigen-admittances are calculated to be

$$\mathbf{\Lambda} = \mathrm{diag}\{a-d, a+d, a-d, a-d, a+d, a+d\} \quad (17)$$

$$a - d = -j\frac{\cot\frac{\varphi_0}{2}}{Z_0} \quad (18)$$

$$a + d = j\frac{\tan\frac{\varphi_0}{2}}{Z_0}. \quad (19)$$

This means the following equations should be satisfied simultaneously for the tri-channel crossover:

$$Y_{ooo} = Y_{oe} \quad (20)$$

$$Y_{eee} = Y_{ee} \quad (21)$$

$$Y_{ooo}Y_{eee} = \frac{1}{Z_0^2}. \quad (22)$$

If the network is lossless, all the eigen-admittances should be purely imaginary numbers, infinities or zeros.

For the central frequency of a tri-channel crossover, there are three independent equations described by (20)–(22). This means at least three independent circuit parameters, such as characteristic impedances and electrical lengths, should be synthesized to achieve the perfect central performance of the tri-channel crossover. If more than three independent variables are provided

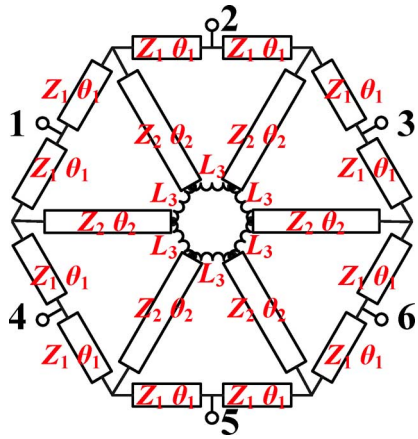

Fig. 4. Schematic of the proposed planar crossover for three channels.

by a certain configuration, other specifications can be considered in the circuit design, which are not limited at the central frequency of the operating band.

III. Six-Port Ring Crossover With Lumped Inductors

A. Configuration and Design Equations

Fig. 4 shows the proposed circuit configuration for the planar tri-channel crossover. It is constructed with a six-port ring structure and six lumped inductors, which are connected through six transmission lines. Obviously, it is a sixfold rotational symmetric structure and its sixth subnetwork is also symmetric to the middle plane of itself. Therefore, the analysis method in Section II can be applied for it. When the values of the characteristic impedances Z_1, Z_2, the electrical lengths θ_1, θ_2, and the inductance L_3 are selected properly, the performance of tri-channel crossover will be achieved.

The partial equivalent circuits are shown in Fig. 5 for the four eigen-admittances. According to Fig. 5(a) and (b), the input admittances Y_{ooo} and Y_{eee} are obtained by

$$Y_{ooo} = -j\frac{2}{Z_1 \tan\theta_1} \tag{23}$$

$$Y_{eee} = j\frac{2}{Z_1}\frac{Z_1 + 2Z_2 \tan\theta_1 \cot\theta_2}{2Z_2 \cot\theta_2 - Z_1 \tan\theta_1}. \tag{24}$$

The admittance matrix of $\mathbf{Y_{oe}}$ is calculated for the two-port subnetwork in Fig. 5(c), and then the eigen-admittance Y_{oe} is obtained with (7) to be

$$Y_{oe} = j\frac{2\cos 2\theta_1 - AZ_1 \sin 2\theta_1 - 1}{Z_1^2 A \sin^2\theta_1 - Z_1 \sin 2\theta_1} \tag{25a}$$

$$A = \frac{X_L \tan\theta_2 - Z_2}{Z_2(X_L + Z_2 \tan\theta_2)} \tag{25b}$$

where $X_L = \omega L_3$ is the reactance of the inductor. According to Fig. 5(d) and (10), the eigen-admittance Y_{ee} is derived by

$$Y_{ee} = -j\frac{(2B\cos\theta_1 + 1)Z_1 \sin\theta_1 + C(4\cos^2\theta_1 - 1)}{CZ_1 \sin 2\theta_1 + BZ_1^2 \sin^2\theta_1} \tag{26a}$$

$$B = \cos\theta_1(3\cos^2\theta_2 - 2) + \frac{X_L Z_1 \sin\theta_1 \sin^2\theta_2}{2Z_2^2} - \frac{\sin\theta_2 \cos\theta_2(3Z_1 \sin\theta_1 + 2X_L \cos\theta_1)}{2Z_2} \tag{26b}$$

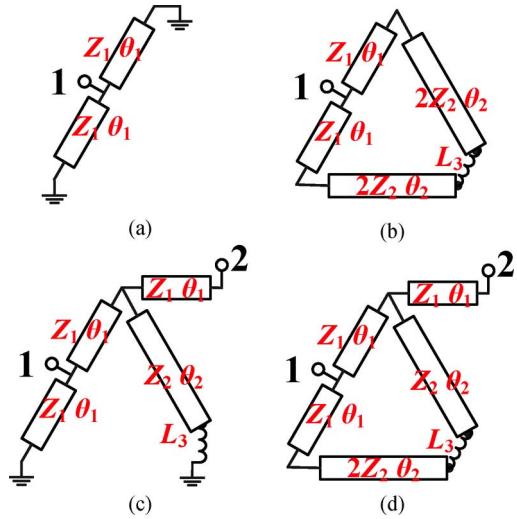

Fig. 5. Partial equivalent circuits of the proposed planar crossover for the four eigen-admittances: (a) Y_{ooo}, (b) Y_{eee}, (c) Y_{oe}, and (d) Y_{ee}.

$$C = \cos\theta_1 \cos\theta_2(3Z_2 \sin\theta_2 + X_L \cos\theta_2) + \frac{Z_1 \sin\theta_1}{2}(3\cos^2\theta_2 - 1) - \frac{X_L Z_1 \sin\theta_1 \sin\theta_2 \cos\theta_2}{2Z_2}. \tag{26c}$$

Substituting (23)–(26) into (20)–(22), the design equations are constructed for the ideal performances of the tri-channel crossover at the central frequency, including perfect matching for each port, perfect transmission between diagonal ports, and perfect isolation between different signal channels.

Combining (18) and (23), it is found that

$$\varphi_0 = 2\tan^{-1}\frac{Z_1 \tan\theta_1}{2Z_0}. \tag{27}$$

The transmission phase at the central frequency of the crossover is determined by the characteristic impedance and electrical length of the ring.

B. Design Curves and Operating Bandwidth

There are five independent variables $Z_1, Z_2, \theta_1, \theta_2$, and L_3 (or X_L) in our proposed planar crossover to meet the requirement of three design equations (20)–(22). Thus, two of them, i.e., Z_2 and X_L, can be predetermined and then the other three parameters θ_1, θ_2, and Z_1 are solved from (20)–(22).

The related design curves are plotted in Fig. 6, where the values of Z_2 and X_L are selected within the ranges of 30 to 150 Ω and 20 to 200 $\pi\Omega$, respectively. The corresponding solved values of θ_1, θ_2 and Z_1 are almost within 36° to 56°, 100° to 155°, and 30 to 80 Ω, respectively. The realizable region is limited by the allowable characteristic impedances from 30 to 150 Ω, which is marked with a gray line in Fig. 6(a) and (d).

A typical theoretical response of the proposed planar tri-channel crossover is shown in Fig. 7 with $Z_2 = 130\,\Omega$, $X_L = 100\pi\Omega$, $\theta_1 = 53.8°$, $\theta_2 = 112.5°$ and $Z_1 = 58.7\ \Omega$. The transmission phase at the central frequency is $\varphi_0 = 77.5°$. All the losses of transmission lines and inductors are not considered here. It is seen that the ideal crossover characteristic is achieved at the central frequency. The performances of port matching

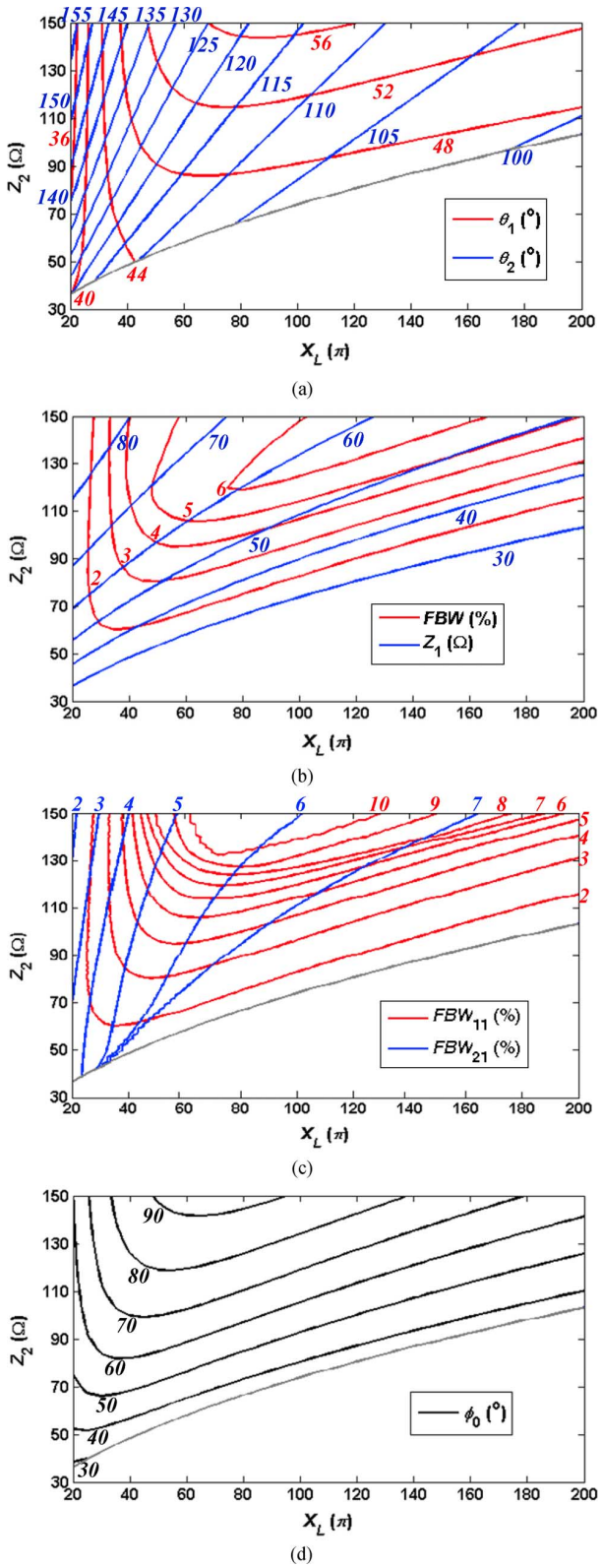

Fig. 6. Solved values with different combinations of Z_2 and X_L for: (a) θ_1 and θ_2, (b) Z_1 and FBW, (c) FBW_{11} and FBW_{21}, and (d) the transmission phase φ_0.

(S_{11}) and isolation between adjacent ports (S_{21}) degrade quickly when away from the central frequency. Thus, only a narrow operating band is obtained when the magnitude lower than -15 dB is required for all the S-parameters, except the

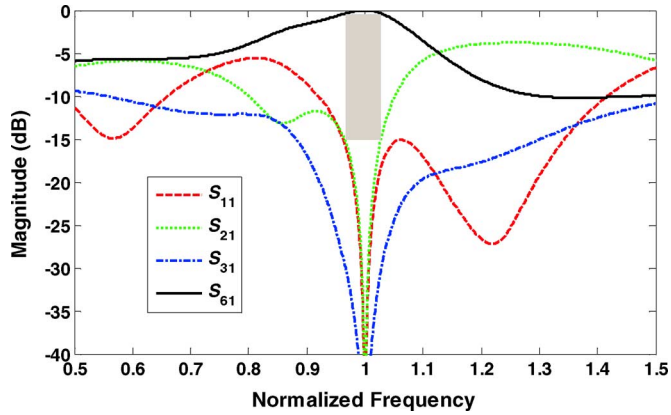

Fig. 7. Theoretical response of the proposed tri-channel crossover with $Z_2 = 130\ \Omega$, $X_L = 100\pi\Omega$, $\theta_1 = 53.8°$, $\theta_2 = 112.5°$ and $Z_1 = 58.7\ \Omega$.

diagonal transmissions, which is marked with gray color in Fig. 7. The normalized frequency of the operating band is from 0.9644 to 1.0276, corresponding to the fractional operating bandwidth (FBW) of 6.32%. The in-band insertion loss of the diagonal transmission is lower than 0.43 dB.

The curves of FBW with the two predetermined parameters of Z_2 and X_L are plotted in Fig. 6(b). Triangle contours are observed in the plane. This is because the simultaneous limitation of S_{11} and S_{21} under -15 dB. The curves of the corresponding fractional bandwidths of FBW_{11} and FBW_{21} are plotted in Fig. 6(c) for comparison. Note that the overall bandwidth FBW of about 1%–6% is smaller than both FBW_{11} and FBW_{21}. When Z_2 is higher than 120 Ω and X_L is around 120 $\pi\Omega$, the preferred response with the FBW over 6% can be achieved, but a small line width is required to realize a very high characteristic impedance, which becomes lossy and sensitive to the fabrication tolerance. Therefore, Z_2 is set around 130 Ω in our design.

According to (27), the transmission phase at the central frequency of the tri-channel crossover is calculated for each set of Z_2 and X_L, as shown in Fig. 6(d). Small Z_2 and X_L correspond to small φ_0. However, if the bandwidth over 6% is desired, the transmission phase should be between 70°–90°. In a realized tri-channel crossover, the additional phase shift introduced by feeding lines should also be taken into account.

C. *Influence of Lumped Inductors*

Although some transmission-line-based planar structures may be utilized to replace the lumped inductors, it is still quite difficult to realize such a high reactance, as in Section III-B. Thus, the lumped inductors are essential elements in our proposed planar crossover. Their characteristics have significant influence on the crossover performance.

First, the Q-factor Q_L of the lumped inductors are usually lower than the Q-factor of transmission-line structures. The lossy inductors will result in relatively high in-band insertion loss in comparison with the circuits without lumped inductors. The diagonal transmission coefficients with different values of Q_L are shown in Fig. 8(a), where the design parameters are the same as those in Fig. 7. The insertion loss increases from 0 to 1.69 dB at the central frequency when Q_L is reduced from infinity to 10. Low-Q inductors will significantly degrade the transmission performance. When $Q_L = 70$, the

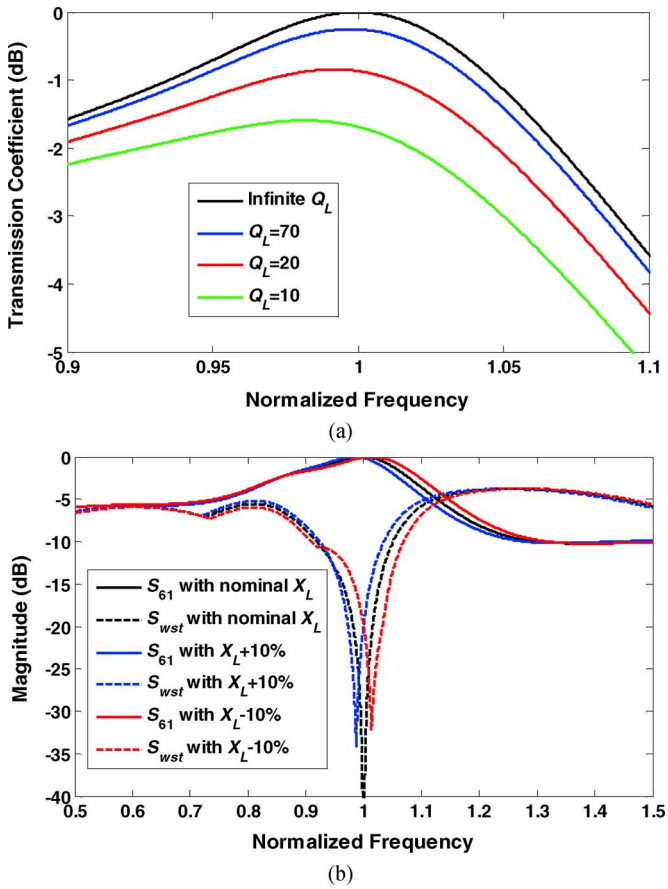

Fig. 8. Influence of lumped inductors on the tri-channel crossover performance, where the parameters are the same as those in Fig. 7. (a) Influence of Q-factor Q_L on the transmission coefficient. (b) Influence of the inductance tolerance on the frequency response.

central insertion loss is about 0.25 dB, which is still acceptable. The fractional bandwidth is almost unchanged with different Q-factors.

The inductance value of the lumped inductors is with a certain tolerance, usually $\pm 2\%$, $\pm 5\%$ or even $\pm 10\%$. The tolerance will introduce frequency shift into the crossover when other parameters are fixed, as shown in Fig. 8(b), where S_{wst} is defined by

$$S_{wst}(\text{dB}) = \max\{S_{11}(\text{dB}), S_{21}(\text{dB}), S_{31}(\text{dB})\}. \qquad (28)$$

The operating band will shift 1.3% to lower or higher frequencies when the reactance of the inductors is 10% larger or smaller than the nominal value, respectively. The fractional bandwidths are 6.32%, 5.28%, and 6.18% with the inductor reactance equal to, 10% larger than and 10% smaller than the nominal value, respectively. In other words, although the inductance tolerance has small influence on the central operating frequency, the bandwidth will be reduced considerably when the inductance is larger than its designed value.

Another limitation introduced by the lumped inductors is the operating frequency, which cannot exceed the self-resonant frequency (SRF) of the used inductors. For example, the 0302CS-7N2XJL chip inductor [34] from Coilcraft Inc. has the nominal inductance of 7.2 nH and the SRF of 9.12 GHz, which can be used for the operating frequency around $f_0 = 7$ GHz. One potential method to solve this problem is to add an additional quarter-wavelength inverter at each port. In this case, the equivalent port impedance Z_0 is reduced, and the values of Z_1, Z_2, and X_L can be reduced accordingly. If Z_1 is set to 35.6 Ω when the equivalent value of Z_0 decreases to 31.8 Ω, X_L will decrease to about $70\pi\Omega$. The Coilcraft 0302CS-3N0XJL inductor [34] with the nominal inductance of 3.0 nH and the SRF of 15.1 GHz can then be applied for the operating frequency up to $f_0 = 12$ GHz, but the additional inverters will increase the occupied area and losses. Further investigation should also be carried out to extend the applicable frequency of the proposed planar tri-channel crossover to beyond X-band.

According to the above analysis, it can be concluded that the lumped inductors with both high Q-factor and small tolerance are desired in our design of tri-channel crossover. If a high operating frequency is demanded, the high SRF should also be provided.

D. Design Procedure

The proposed planar crossover for three intersecting signal channels can be designed according to the following steps.

Step 1) Select the lumped inductors properly to make the reactance $X_L = 2\pi f_0 L_3$ within the range of $[80\pi\Omega, 115\pi\Omega]$ at the desired central frequency f_0. The characteristic impedance Z_2 can be set around 130 Ω for relatively large operating bandwidth.

Step 2) Find the values of the parameters θ_1, θ_2, and Z_1 with the design curves in Fig. 6, or solve them by using (20)–(26).

Step 3) Obtain the initial values for the widths, w_1 and w_2, and the lengths, l_1 and l_2, of the transmission lines, according to the substrate parameters and the values of Z_1, Z_2, θ_1 and θ_2.

Step 4) Construct the planar crossover structure. In order to reduce the occupied area, the lines may be folded. The pads are also designed for the surface mount of the six lumped inductors with their package sizes.

Step 5) Optimize the layout to consider the influence of discontinuities, losses, and parasitic couplings. The design of the tri-channel crossover is then carried out successfully.

IV. Results and Discussion

A microstrip prototype is developed to validate our design method, as shown in Fig. 9. The specific operating band is centered at $f_0 = 1.0$ GHz. The Rogers RO4003 substrate is used with the relative permittivity of $\varepsilon_r = 3.55$, the loss tangent of $\tan\delta = 0.0027$, and the substrate thickness of $h = 32$ mil.

The high-performance ceramic chip inductors with the part number of 0603HP-51NXGLU [35] are selected. The package size of the surface-mounted inductor is about $1.75 \times 0.98 \times 0.94$ mm^3. The nominal value of the inductance tested at 200 MHz is 51 nH with the Q-factor of $Q_L = 49$ and the inductance tolerance of $\pm 2\%$. By using the measured S-parameters provided online [35], it is extracted that the inductance around $f_0 = 1.0$ GHz is about $L_3 = 55.5$ nH with its Q_L higher than 70. The reactance is then $X_L = 111\pi\Omega$ at

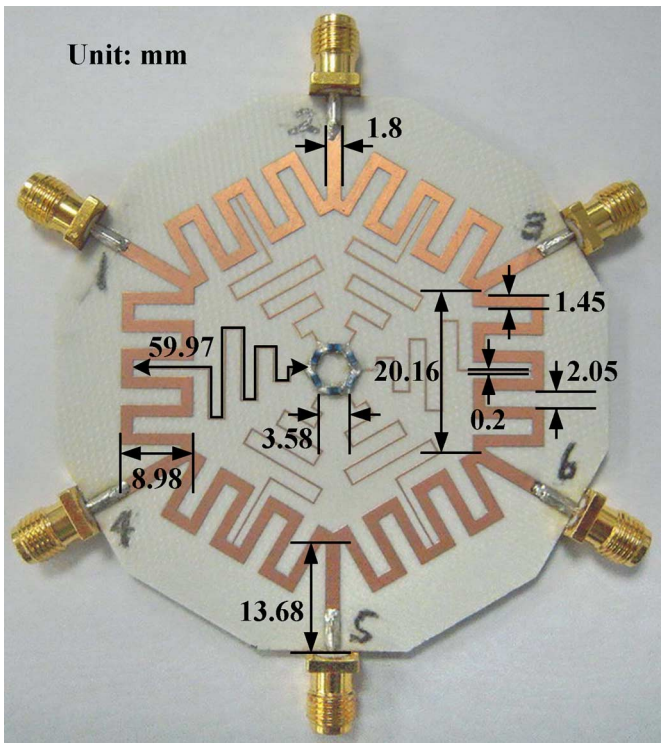

Fig. 9. Photograph of the proposed planar tri-channel crossover prototype.

1.0 GHz, but the tolerance of the inductance value at 1.0 GHz is not clear.

The characteristic impedance Z_2 is set to 128.7 Ω, which is corresponding to the width $w_2 = 0.2$ mm of the microstrip line. The values of Z_1, θ_1, and θ_2 are synthesized to be 55.9 Ω, 53.2°, and 110.3°, respectively. The synthesized transmission phase and bandwidth are $\varphi_0 = 73.5°$ and FBW $= 6.04\%$, respectively. The initial circuit geometry is then determined with $w_1 = 1.49$ mm, $l_1 = 26.8$ mm, and $l_2 = 58.7$ mm. Both the ring and loading stubs are implemented with meandering lines. The layout is optimized with the full-wave simulator ANSYS HFSS. The critical physical dimensions have been shown in Fig. 9. The overall size of the planar tri-channel crossover, except for the feeding lines, is 55.3×52.9 mm^2, i.e., $0.308 \times 0.294\lambda_g^2$, where λ_g is the guided wavelength of 50-Ω microstrip line at the central frequency $f_0 = 1.0$ GHz.

The prototype is measured by a four-port vector network analyzer, R&S ZVA50. The other two ports of the crossover is matched with two broadband loads. The theoretical, full-wave simulated, and measured results are given in Fig. 10. The theoretical responses are obtained for the ideal lossless case. Reasonable agreement is observed between the theoretical and simulated results. The simulated central frequency of 0.99 GHz is especially close to the designed value of 1.0 GHz in theory. The difference between them is due to the discontinuities and parasitic couplings in the full-wave simulated model.

The measured results agree well with the simulated results, except that the measured response shifts 37 MHz to higher frequency. The frequency shift should be mainly due to the tolerance of layout fabrication and substrate parameters since even the 10% inductance tolerance will only lead to a shift of 1.3%, as indicated in Section III-C. Since the narrowest line width w_2 is only 0.2 mm, its tolerance may have the most obvious influence on the component performance. Fig. 11 shows the influence of w_2 on S_{61} and S_{wst} by full-wave simulations, where

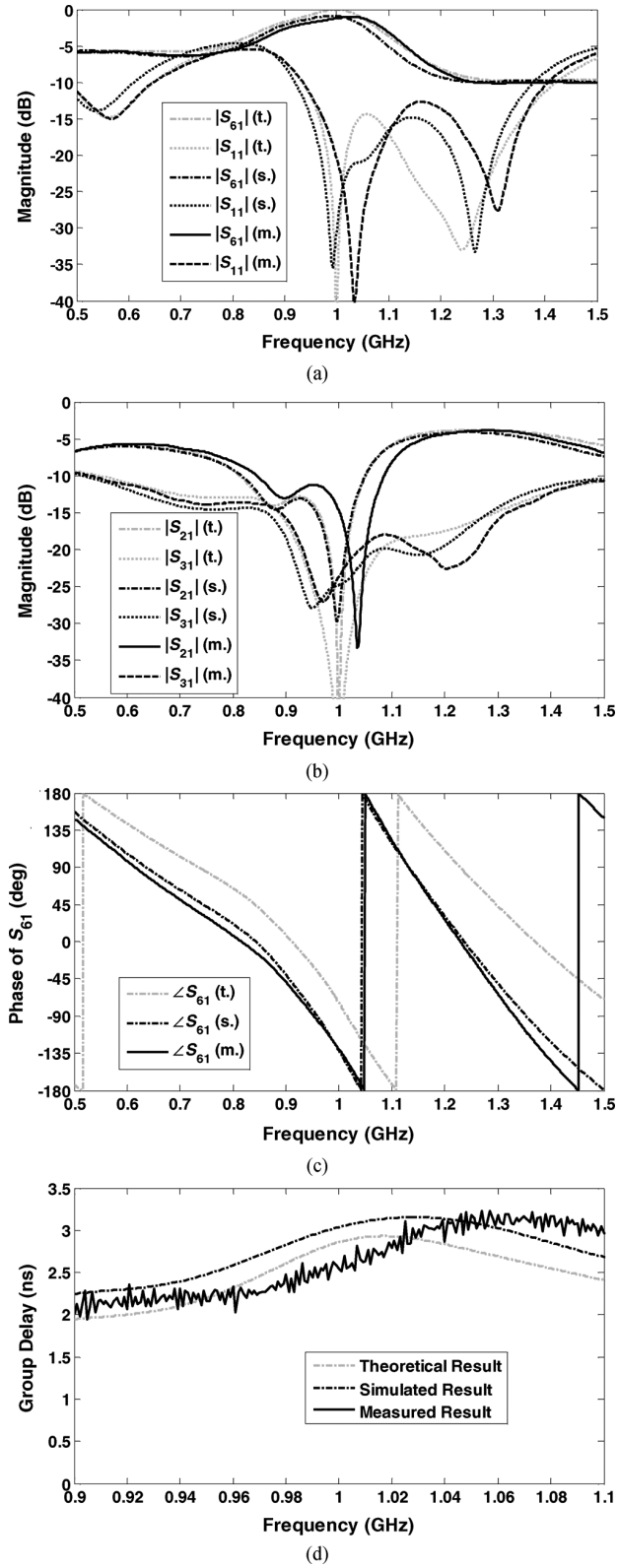

Fig. 10. Theoretical (t.), simulated (s.), and measured (m.) results of the proposed tri-channel crossover prototype. (a) Magnitudes of the reflection S_{11} and the diagonal transmission S_{61}. (b) Magnitudes of the isolations S_{21} and S_{31} between different signal channels. (c) Phase of S_{61}. (d) Group delay of the diagonal transmission S_{61}.

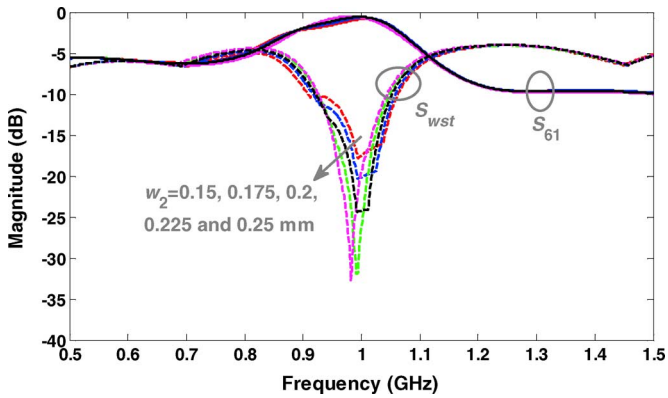

Fig. 11. Simulated tolerance influence of the line width w_2 on S_{61} and S_{wst}, where the fabrication tolerance is set to ± 0.025 and ± 0.05 mm.

the fabrication tolerance is set to ± 0.025 mm (1 mil) and ± 0.05 mm (2 mil), according to the standard PCB process. When w_2 is accurately set to 0.2 mm, the -15-dB band is from 0.965 to 1.029 GHz, with the central frequency of 0.997 GHz and the bandwidth of 64 MHz. For $w_2 = 0.15$ mm, the central frequency is 1.012 GHz and the bandwidth is 56 MHz. For $w_2 = 0.25$ mm, the central frequency becomes 0.984 GHz and the bandwidth is 68 MHz. It can be concluded that smaller w_2 will result in the operating band shifted to higher frequency with a narrower bandwidth while larger w_2 will result in the operating band shifted to lower frequency with a little wider bandwidth. The frequency shift and the change of bandwidth, due to the fabrication tolerance ± 0.05 mm of the line width w_2 for the standard PCB technology, are within ± 16 and ± 8 MHz, respectively.

The measured central insertion loss is 1.0 dB, only 0.15 dB higher than the simulated value, which is introduced by the SMA connectors used in measurement. The relatively large insertion loss is mainly resulted from the utilization of narrow microstrip line and lumped inductors. The magnitudes of S_{11} and S_{21} are both lower than -30 dB at 1.03 GHz while the magnitude of S_{31} is lower than -20 dB there. The measured operating band of 61 MHz is limited within 1.0–1.06 GHz, mainly due to the degeneration of the isolation performance between two adjacent ports. The in-band insertion loss is better than 1.4 dB.

Fig. 12 shows the simulated electric field distribution of the tri-channel crossover prototype at 1.0 GHz, where only the signal channel between Ports 2 and 5 is on work. It is seen that almost no power couples to the other ports, which corresponds to the good channel isolations of $|S_{21}|$ and $|S_{31}|$ in Fig. 10(b). The electric field shows the distribution of traveling wave on the feeding lines, indicating that good port matching is achieved.

From Fig. 10(c), it can be seen that the simulated and measured phases of S_{61} agree well with each other around the operating band. The deviation from the theoretical phase is caused by the additional feeding lines. The group delay of the diagonal transmission is also an important characteristic of the planar crossover. The measured result from 0.9 to 1.1 GHz is shown in Fig. 10(d), with the theoretical and simulated results given for comparison. The simulated group delay is about 0.3 ns larger than the theoretical one within the whole frequency range of interest, which mainly comes from the feeding lines. The

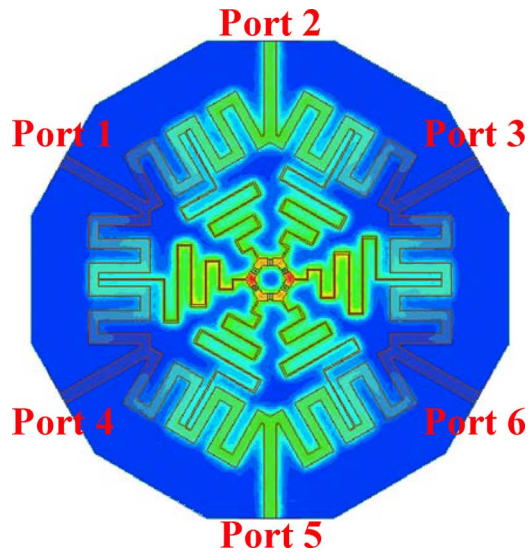

Fig. 12. Simulated electric field distribution of the tri-channel crossover prototype at 1.0 GHz where only the channel between Ports 2 and 5 is on work.

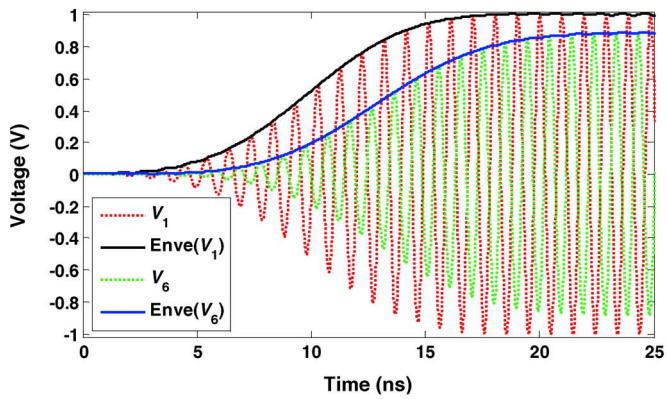

(a)

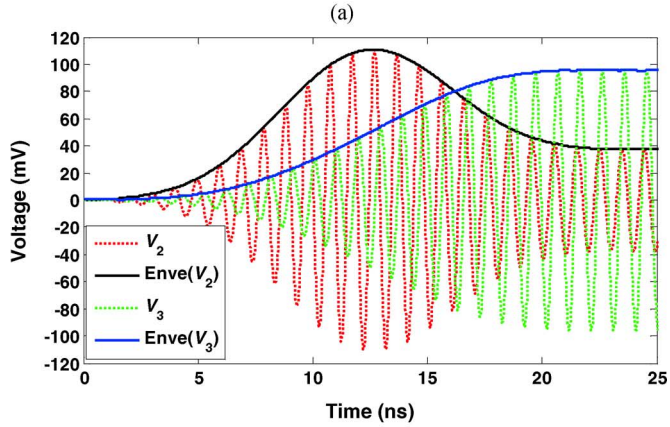

(b)

Fig. 13. Time-domain simulated voltages and their envelopes (Enve) with the measured S-parameters of the prototype. (a) V_1 and V_6. (b) V_2 and V_3.

frequency shift is also observed from the difference between the simulated and measured group delays. In measurement, the in-band group delay is from 2.5 to 3.2 ns. The variation of 0.7 ns is much smaller than the period of 16.4 ns corresponding to the measured bandwidth of 61 MHz.

In order to show how the signal is transmitted in one channel with efficiently suppressed leakage to the other two channels, the time-domain simulation is carried out with the

measured S-parameters of the crossover prototype. As shown in Fig. 13(a), an Gaussian-shaped step signal V_1 enters Port 1, whose rise time, carrier frequency and envelope amplitude are 20 ns, 1.03 GHz, and 1 V, respectively. It is clearly seen that the voltage envelope of the signal V_6 received at Port 6 is delayed by about 3 ns, whose amplitude is 0.89 V. These agree well with the measured in-band insertion loss and group delay of S_{61} in the frequency domain. The steady-state amplitudes of V_2 and V_3 are lower than 40 and 100 mV, which correspond to the suppressions of 30 and 20 dB at the central frequency 1.03 GHz for S_{21} and S_{31}, respectively. However, there is an overshoot in the time-domain response of V_2 before reaching the steady state. This is because the rejection band of S_{21} is limited, which makes V_2 sensitive to the other frequency components in the rising edge, but note that the peak amplitude of V_2 is still not higher than 110 mV. Therefore, the channel transmission and isolation have been successfully achieved with our proposed tri-channel crossover.

V. Conclusion

A planar crossover is proposed in this paper for three intersecting channels. The component is a sixfold rotational symmetric structure based on a stub-loaded ring and six lumped inductors. It is analyzed by using the eigen-admittances and the even-/odd-mode theory. Design curves are plotted to determine the critical parameters, including characteristic impedances, electrical lengths, and inductance for the specific central frequency and an operating bandwidth over 6%. The influence of Q-factor and tolerance of lumped inductors on the crossover performance is explored. In order to validate our idea, a microstrip prototype is developed at 1.0 GHz with the fractional bandwidth of 6% and the occupied area of $0.308 \times 0.294\lambda_g^2$. The performances of diagonal transmission, port matching, and isolation between different channels are demonstrated by the theoretical, simulated, and measured results.

Acknowledgment

The authors appreciate Coilcraft Singapore Pte Ltd.. Sinagpore, for providing the high-performance chip inductor samples.

References

[1] T.-S. Horng, "A rigorous study of microstrip crossovers and their possible improvements," *IEEE Trans. Microw. Theory Techn.*, vol. 42, no. 9, pp. 1802–1806, Sep. 1994.

[2] G. E. Ponchak and E. M. Tentzeris, "Finite ground coplanar waveguide (FGC) low loss, low coupling 90-degree crossover junctions," *IEEE Trans. Adv. Packag.*, vol. 25, no. 3, pp. 385–392, Aug. 2002.

[3] K. U-yen, E. J. Wollack, S. H. Moseley, T. R. Stevenson, W.-T. Hsieh, and N. T. Cao, "Via-less microwave crossover using microstrip-CPW transitions in slotline propagation mode," in *IEEE MTT-S Int. Microw. Symp. Dig.*, Boston, MA, USA, Jun. 2009, pp. 1029–1032.

[4] W.-D. Liu, Z.-J. Zhang, Z.-H. Feng, and M. F. Iskander, "A compact wideband microstrip crossover," *IEEE Microw. Wireless Compon. Lett.*, vol. 22, no. 5, pp. 254–256, May 2012.

[5] A. M. Abbosh, "Wideband planar crossover using two-port and four-port microstrip to slotline transitions," *IEEE Microw. Wireless Compon. Lett.*, vol. 22, no. 9, pp. 465–467, Sep. 2012.

[6] J. S. Wight, W. J. Chudobiak, and V. Makios, "A microstrip and stripline crossover structure," *IEEE Trans. Microw. Theory Techn.*, vol. MTT-24, no. 5, p. 270, May 1976.

[7] F. C. de Ronde, "Octave-wide matched symmetrical, reciprocal, 4- and 5-ports," in *IEEE MTT-S Int. Microw. Symp. Dig.*, Dallas, TX, USA, Jun. 1982, pp. 521–523.

[8] Y.-C. Chiou, J.-T. Kuo, and H.-R. Lee, "Design of compact symmetric four-port crossover junction," *IEEE Microw. Wireless Compon. Lett.*, vol. 19, no. 9, pp. 545–547, Sep. 2009.

[9] F. Tefiku and E. Yamashita, "Improved analysis method for multiport microstrip annular-ring power-dividers," *IEEE Trans. Microw. Theory Techn.*, vol. 42, no. 3, pp. 376–382, Mar. 1994.

[10] D. V. Kholodniak and I. B. Vendik, "A novel type of 0-dB directional coupler for microwave integrated circuits," in *29th Eur. Microw. Conf.*, Munich, Germany, Oct. 1999, vol. 2, pp. 341–344.

[11] D. Kholodniak, G. Kalinin, E. Vernoslova, and I. Vendik, "Wideband 0-dB branch-line directional couplers," in *IEEE MTT-S Int. Microw. Symp. Dig.*, Boston, MA, USA, Jun. 2000, vol. 3, pp. 1307–1310.

[12] J.-J. Yao, C. Lee, and S.-P. Yeo, "Microstrip branch-line couplers for crossover application," *IEEE Trans. Microw. Theory Techn.*, vol. 59, no. 1, pp. 87–92, Jan. 2011.

[13] T. Bechteler, B. Mayer, and R. Weigel, "A new high-temperature superconducting double-hybrid coupler with wide bandwidth," in *IEEE MTT-S Int. Microw. Symp. Dig.*, Denver, CO, USA, Jun. 1997, vol. 1, pp. 311–314.

[14] X. Liu, C.-P. Yu, Y.-A. Liu, S.-L. Li, F. W. Fan, and M. Su, "A novel compact planar crossover with simple design procedure," in *Proc. Asia–Pacific Microw. Conf.*, Yokohama, Japan, Dec. 2010, pp. 1633–1636.

[15] Y. Chen and S.-P. Yeo, "A symmetrical four-port microstrip coupler for crossover application," *IEEE Trans. Microw. Theory Techn.*, vol. 55, no. 11, pp. 2434–2438, Nov. 2007.

[16] Y.-C. Chiou, C.-H. Tsai, and J.-T. Kuo, "Comments on 'a symmetrical four-port microstrip coupler for crossover application'," *IEEE Trans. Microw. Theory Techn.*, vol. 57, no. 7, pp. 1859–1860, Jul. 2009.

[17] Y.-C. Chiou, S.-W. Lai, and J.-T. Kuo, "Analysis and design of double-ring crossover junction with arbitrary diagonal port impedances," in *Proc. Asia–Pacific Microw. Conf.*, Singapore, Singapore, Dec. 2009, pp. 2092–2095.

[18] E. Gandini, M. Ettorre, R. Sauleau, and A. Grbic, "A lumped-element unit cell for beam-forming networks and its application to a miniaturized Butler matrix," *IEEE Trans. Microw. Theory Techn.*, vol. 61, no. 4, pp. 1477–1487, Apr. 2013.

[19] B. Henin and A. Abbosh, "Design of compact planar crossover using Sierpinski carpet microstrip patch," *IET Microw. Antennas Propag.*, vol. 7, no. 1, pp. 54–60, Jan. 2013.

[20] Y.-F. Wang, A. M. Abbosh, and B. Henin, "Broadband microwave crossover using combination of ring resonator and circular microstrip patch," *IEEE Trans. Compon. Packag. Manuf. Technol.*, vol. 3, no. 10, pp. 1771–1777, Oct. 2013.

[21] F.-L. Wong and K.-K. M. Cheng, "A novel, planar, and compact crossover design for dual-band applications," *IEEE Trans. Microw. Theory Techn.*, vol. 59, no. 3, pp. 568–573, Mar. 2011.

[22] S. Yeung, W.-C. Ip, and K.-K. M. Cheng, "A novel dual-band crossover design with enhanced frequency band ratio and operating bandwidth," in *Proc. Asia–Pacific Microw. Conf.*, Melbourne, Australia, Dec. 2011, pp. 892–895.

[23] Z.-W. Lee and Y.-H. Pang, "Compact planar dual-band crossover using two-section branch-line coupler," *Electron. Lett.*, vol. 48, no. 21, pp. 1348–1349, Oct. 2012.

[24] F. Lin, Q.-X. Chu, and S.-W. Wong, "Dual-dand planar crossover with two-section branch-line structure," *IEEE Trans. Microw. Theory Techn.*, vol. 61, no. 6, pp. 2309–2316, Jun. 2013.

[25] J. Shao, H. Ren, B. Arigong, C.-Z. Li, and H.-L. Zhang, "A fully symmetrical crossover and its dual-frequency application," *IEEE Trans. Microw. Theory Techn.*, vol. 60, no. 8, pp. 2410–2416, Aug. 2012.

[26] F. Gardiol, *Microstrip Circuits*. New York, NY, USA: Wiley, 1994.

[27] G. F. Engen, "The six-port reflectometer: An alternative network analyzer," *IEEE Trans. Microw. Theory Techn.*, vol. MTT-25, no. 12, pp. 1075–1080, Dec. 1977.

[28] G. P. Riblet and E. R. B. Hansson, "Some properties of the matched, symmetrical six-port junction," *IEEE Trans. Microw. Theory Techn.*, vol. MTT-32, no. 2, pp. 164–171, Feb. 1984.

[29] S.-P. Yeo, "Analysis of symmetrical six-port junction when configured as a six-port reflectometer," *IEEE Trans. Instrum. Meas.*, vol. 41, no. 2, pp. 193–197, Apr. 1992.

[30] S. Judah, M. J. Page, and M. Judd, "Planar symmetrical six-port junction," *Proc. IEE*, vol. 134, no. 2, pp. 109–115, Apr. 1987.
[31] S.-P. Yeo, B. Tan, and E.-H. Kwek, "Improved design for symmetrical six-port microstrip coupler (based on double-ring-with-star topology)," *IEEE Trans. Microw. Theory Techn.*, vol. 48, no. 6, pp. 1074–1077, Jun. 2000.
[32] Y. Chen, J.-J. Yao, and S.-P. Yeo, "Matched symmetrical six-port microstrip coupler," in *IEEE MTT-S Int. Microw. Symp. Dig.*, Boston, MA, USA, Jun. 2005, pp. 1223–1226.
[33] J.-C. Coetzee and Y.-T. Yu, "Design of decoupling networks for circulant symmetric antenna arrays," *IEEE Antennas Wireless Propag. Lett.*, vol. 8, pp. 291–294, 2009.
[34] "The online data of the Coilcraft ceramic chip inductors (0302CS)," Coilcraft, Cary, IL, USA, 2014. [Online]. Available: http://www.coilcraft.com/0302cs.cfm
[35] "The online data of the Coilcraft ceramic chip inductors (0603HP)," Coilcraft, Cary, IL, USA, 2013. [Online]. Available: http://www.coilcraft.com/0603hp.cfm

Lin-Sheng Wu (S'09–M'10) was born in 1981. He received the B.S. degree in electronic and information engineering, and the M.S. and Ph.D. degrees in electromagnetic fields and microwave technologies from Shanghai Jiao Tong University (SJTU), Shanghai, China, in 2003, 2006, and 2010, respectively.

From August to November 2010 and December 2012 to December 2013, he was a Research Fellow with the Department of Electrical and Computer Engineering, National University of Singapore (NUS), Sinapore. From February 2010 to January 2012, he was a Post Doctor with SJTU. He is currently a Lecturer with the Key Laboratory of Ministry of Education of Design and Electromagnetic Compatibility of High Speed Electronic Systems in SJTU. He has authored or coauthored approximately 80 technical papers. His current research interest is mainly focused on novel techniques for microwave integration, passive components, and carbon nanoelectronics.

Dr. Wu was a session co-chair of the Asia–Pacific Microwave Conference (APMC) and the IEEE Electrical Design of Advanced Packaging and Systems Symposium (EDAPS) in 2011. He is a reviewer of several international journals, including four publications.

Yong-Xin Guo (S'00–A'02–M'03–SM'05) received the Ph.D. degree from the City University of Hong Kong, Hong Kong, in 2001.

He is currently an Associate Professor with the Department of Electrical and Computer Engineering (ECE), National University of Singapore (NUS), Singapore, and Director of the Center for Microwave and Radio Frequency of the Department of ECE, NUS. Concurrently, he is a Senior Investigator with the National University of Singapore Research Institute (NUSRI), Suzhou, China, and Director of the Center of Advanced Microelectronic Devices, NUSRI. From September 2001 to January 2009, he was with the Institute for Infocomm Research, Singapore, as a Research Scientist. He has authored or coauthored 132 international journal papers and 150 international conference papers. His publications have been cited by others more than 1040 times (source: Scopus). He holds one Chinese Patent, one U.S. patent and four provisional U.S. patents. His current research interests include microstrip antennas for wireless communications, implantable/wearable antennas and body channel modeling for medical applications, wireless power and RF energy harvesting, microwave circuits, and monolithic microwave integrated circuit (MMIC) modeling and design.

Dr. Guo was the general chair of the IEEE Microwave Theory and Techniques Society (MTT-S) International Microwave Workshop Series 2013 on "RF and Wireless Technologies for Biomedical and Healthcare Applications" (IMWS-Bio 2013), Singapore. He is an associate editor for IEEE ANTENNAS AND WIRELESS PROPAGATION LETTERS (AWPL). He was a recipient of the Young Investigator Award 2009, National University of Singapore and the 2013 "Raj Mittra" Travel Grant Senior Researcher Award.

Jun-Fa Mao (M'92–SM'98–F'12) was born in 1965. He received the B.S. degree in radiation physics from the University of Science and Technology of National Defense, Changsha, Hunan Province, China, in 1985, the M.S. degree in experimental nuclear physics from the Shanghai Institute of Nuclear Research, Shanghai, China, in 1988, and the Ph.D. degree in electronic engineering from Shanghai Jiao Tong University, Shanghai, China, in 1992.

Since 1992, he has been a faculty member with Shanghai Jiao Tong University, where he is currently a Chair Professor and the Executive Dean of the School of Electronic, Information and Electrical Engineering. From 1994 to 1995, he was a Visiting Scholar with the Chinese University of Hong Kong, Hong Kong. From 1995 to 1996, he was a Postdoctoral Researcher with the University of California at Berkeley. He is a Chief Scientist of the National Basic Research Program (973 Program) of China, a Project Leader of the National Science Foundation for Creative Research Groups of China, a Cheung Kong Scholar of the Ministry of Education, China, and an Associate Director of the Microwave Society of China Institute of Electronics. He has authored or coauthored over 200 journal papers (including 80 IEEE journal papers) and 120 international conference papers. His research interests include the interconnect and package problem of integrated circuits and systems, analysis, and design of microwave circuits.

Dr. Mao was the 2007–2009 chair of the IEEE Shanghai Section and the 2009–2011 chair of the IEEE Microwave Theory and Techniques Society (IEEE MTT-S) Shanghai Chapter. He was the recipient of the National Natural Science Award of China in 2004, the National Technology Invention Award of China in 2008, the National Science and Technology Progress Award of China in 2012, and the Best Paper Award of the 2008 Symposium of APEMC in conjunction with the 19th International Symposium of Zurich EMC.